Title

The conserved XPF:ERCC1-like Zip2:Spo16 complex controls meiotic crossover formation through structure-specific DNA binding

Journal

Nucleic Acids Research, 47(5)

ISSN

0305-1048

Authors

Arora, Kanika
Corbett, Kevin D

Publication Date

2019-03-18

DOI

10.1093/nar/gky1273

Peer reviewed

Published online 19 December 2018 *Nucleic Acids Research, 2019, Vol. 47, No. 5* **2365–2376**
doi: 10.1093/nar/gky1273

The conserved XPF:ERCC1-like Zip2:Spo16 complex controls meiotic crossover formation through structure-specific DNA binding

Kanika Arora[1] and Kevin D. Corbett[1,2,*]

[1]Department of Cellular and Molecular Medicine, University of California, San Diego, La Jolla, CA 92093, USA and [2]Department of Chemistry and Biochemistry, University of California, San Diego, La Jolla, CA 92093, USA

Received August 09, 2018; Revised December 06, 2018; Editorial Decision December 10, 2018; Accepted December 11, 2018

ABSTRACT

In eukaryotic meiosis, generation of haploid gametes depends on the formation of inter-homolog crossovers, which enable the pairing, physical linkage, and eventual segregation of homologs in the meiosis I division. A class of conserved meiosis-specific proteins, collectively termed ZMMs, are required for formation and spatial control of crossovers throughout eukaryotes. Here, we show that three *Saccharomyces cerevisiae* ZMM proteins—Zip2, Zip4 and Spo16—interact with one another and form a DNA-binding complex critical for crossover formation and control. We determined the crystal structure of a Zip2:Spo16 subcomplex, revealing a heterodimer structurally related to the XPF:ERCC1 endonuclease complex. Zip2:Spo16 lacks an endonuclease active site, but binds specific DNA structures found in early meiotic recombination intermediates. Mutations in multiple DNA-binding surfaces on Zip2:Spo16 severely compromise DNA binding, supporting a model in which the complex's central and HhH domains cooperate to bind DNA. Overall, our data support a model in which the Zip2:Zip4:Spo16 complex binds and stabilizes early meiotic recombination intermediates, then coordinates additional factors to promote crossover formation and license downstream events including synaptonemal complex assembly.

INTRODUCTION

Sexual reproduction in eukaryotes requires the production of haploid gametes in a specialized cell-division program called meiosis, followed by the fusion of two gametes to generate diploid offspring. The reduction of ploidy in meiosis is enabled by the formation of crossovers or chiasmata, specific inter-homolog recombination events that physically link homologs and enable their segregation in the meiosis I division. Because of their importance for accurate chromosome segregation, the formation of crossovers (COs) is subject to tight spatial and temporal regulation: overlapping feedback pathways ensure that each homolog pair receives at least one CO, and that the overall number of COs is kept within a tight range. Most COs are also subject to 'interference'; that is, they are spaced farther apart along chromosomes than expected by random chance, implying a regulatory mechanism that communicates the status of recombination along chromosomes (1,2). Defects in the production or spatial regulation of COs can lead to chromosome mis-segregation and aneuploidy, a major cause of miscarriage and developmental disorders in humans (3,4).

While the molecular machinery that mediates meiotic recombination is highly conserved and well-understood, the regulatory mechanisms controlling the number and spatial distribution of COs are less well-characterized. In the budding yeast *S. cerevisiae*, entry into meiotic prophase is accompanied by assembly of the meiotic chromosome axis, which organizes each pair of replicated sister chromosomes as a linear array of chromatin loops and promotes the formation of DNA double-strand breaks (DSBs) along each chromosome by the Spo11 endonuclease (5–11). These DSBs are resected to free 3′ single-stranded ends and loaded with two related recombinases, Rad51 and Dmc1, which mediate the invasion of a homologous DNA duplex to form a single-end invasion or D-loop intermediate (12,13). In meiotic prophase, use of the identical sister chromatid as a repair template is strongly inhibited by the chromosome axis, thereby promoting invasion of the homolog instead (8,14–19). After initial invasion of the homolog and formation of a D-loop, several competing pathways vie to determine the fate of this early recombination intermediate. Often, the D-loop is dissolved by the combined action of DNA topoisomerases and helicases (in *S. cerevisiae*, the Sgs1, Top3 and Rmi1 proteins) (20–22). If the free 3′ end has undergone new DNA synthesis past the original break, it may re-anneal with the other broken end and be repaired to give a non-crossover (NCO); this pathway is referred to

*To whom correspondence should be addressed. Tel: +1 858 534 7267; Fax: +1 858 534 7750; Email: kcorbett@ucsd.edu

as synthesis-dependent strand annealing (SDSA) and is responsible for the bulk of NCO formation (23,24). A subset of strand invasion intermediates are further processed into double Holliday Junction (dHJ) intermediates (24–26), which may become either COs or NCOs. Type 1 'interfering' COs are generated by specific cleavage of dHJs by the Mlh1:Mlh3 endonuclease (27,28). A minor competing pathway involving non-specific endonucleases (in *S. cerevisiae*, Mus81:Mms4, Yen1 and Slx1:Slx4) can generate either NCOs or type 2 'noninterfering' COs (22,27–31).

The formation of type 1 COs is tightly regulated by a group of proteins collectively termed 'ZMM' proteins after their gene names in *S. cerevisiae*: Zips (Zip1/Zip2/Zip3/Zip4), Msh4:Msh5, and Mer3 (32). Most ZMM proteins are conserved throughout eukaryotes, and their roles in promoting CO formation are generally well-outlined: for example, Mer3 is a DNA helicase (33) and Msh4:Msh5, relatives of the MutS family DNA mismatch recognition proteins, are proposed to bind and stabilize a branched recombination intermediate and recruit the Mlh1:Mlh3 endonuclease for specific dHJ cleavage (34,35). Zip3 is related to ubiquitin/SUMO E3 ligase proteins (36), and as such likely has a role in regulation of protein complex formation or degradation at crossover sites (37,38). Zip1 is the major component of 'transverse filaments' within the synaptonemal complex, a conserved structure that nucleates at initial homolog interaction sites including centromeres and recombination sites, then extends to bring each homolog pair into close juxtaposition along their lengths (39,40). The synaptonemal complex is important for the resolution of crossovers (39–41) and its assembly is also coordinated with removal of Hop1 from the axis by the AAA+ ATPase Pch2 (42–45), an important feedback mechanism that limits further DSB and CO formation.

Of the identified ZMM proteins in *S. cerevisiae*, the roles of Zip2, Zip4 and their more recently-identified binding partner Spo16 are the least well-understood. These three proteins localize to recombination sites on meiotic chromosomes (46,47) and depend on one another for chromosome localization (48,49), suggesting that they act together as a complex. All three proteins are required for wild-type levels of COs (47–50), *zip2* and *zip4* mutants show defects in crossover interference (48,51), and *spo16* and *zip2* mutants also show defects in the formation of single-end invasion/D-loop and dHJ recombination intermediates (49,52). Together, these data suggest that Zip2, Zip4 and Spo16 may directly promote the formation of type 1 COs, potentially by aiding the formation of early recombination intermediates or stabilizing these intermediates against disassembly. Similar findings that both the *A. thaliana* and mammalian Zip2 homologs (both called SHOC1) are required for wild-type levels of crossovers in these organisms (53,54) suggest that a Zip2-containing complex is a highly-conserved and critical player in meiotic CO formation throughout eukaryotes.

In addition to their effects on meiotic recombination, Zip2, Zip4 and Spo16 also play a key role in synaptonemal complex assembly: in mutants of all three genes, the synaptonemal complex protein Zip1 forms foci at recombination sites, but does not then extend along chromosomes to form the full synaptonemal complex (47–49). Zip2 and Zip4 have also been observed to localize at the ends of Zip1 stretches, both on synapsed chromosomes and on extra-chromosomal Zip1 assemblies termed polycomplexes (47,48). Recently, mass spectrometry of Zip2:Zip4:Spo16 complexes purified from meiotic cells has indicated that these proteins directly or indirectly interact with the chromosome axis proteins Hop1 and Red1, the axis remodeler Pch2, and the Msh4:Msh5 complex (55). Overall, these findings suggest that Zip2, Zip4 and Spo16 interact with other ZMMs as well as both chromosome axis and synaptonemal complex proteins, and thereby play a central role in coordinating CO formation with chromosome axis remodeling and synaptonemal complex assembly.

Saccharomyces cerevisiae Zip2 and its homologs in *Arabidopsis thaliana* (AI481877/SHOC1/ZIP2H) and mammals (C9ORF84/SHOC1) show weak homology to XPF, a structure-specific endonuclease that plays important roles in nucleotide excision repair with its binding partner, ERCC1 (55,56). More recently, De Muyt *et al*. found that Spo16 binds the XPF-like domain of Zip2 specifically and shows weak homology to ERCC1, suggesting that these proteins may form a XPF:ERCC1-like complex (55). Here, we outline the architecture of the *S. cerevisiae* Zip2:Zip4:Spo16 complex and show by x-ray crystallography that Zip2 and Spo16 indeed form an XPF:ERCC1-like heterodimer. Zip2:Spo16 lacks an endonuclease active site, suggesting that it instead binds specific DNA structures and nucleates assembly of a larger regulatory complex, similar to the related FANCM:FAAP24 DNA repair complex (57). We show that, like XPF:ERCC1, Zip2:Spo16 can bind a variety of DNA structures, including single-strand/double-strand DNA junctions with the geometry found in meiotic strand-invasion intermediates, and branched/bent DNA structures. We propose a model in which the Zip2:Zip4:Spo16 complex cooperates with Msh4:Msh5 to recognize and stabilize early recombination intermediates, recruit downstream crossover factors to promote the formation of type 1 COs, and coordinate the formation of COs with assembly of the synaptonemal complex.

MATERIALS AND METHODS

For key resources, see Supplementary Table S2.

Yeast two-hybrid assays

For yeast two-hybrid assays, individual proteins were cloned into pBridge and pGADT7 AD vectors (Clontech) with multiple-cloning sites modified for ligation-independent cloning (http://qb3.berkeley.edu/macrolab/lic-cloning-protocol/). pBridge vectors were transformed into *S. cerevisiae* strain AH109 and selected on SC media lacking tryptophan (-TRP). pGADT7 AD vectors were transformed into *S. cerevisiae* strain Y187 and selected on SC media lacking leucine (-LEU). Haploid strains were mated and diploids selected on SC -TRP/-LEU. Diploid cells were diluted in water and replated onto SC -TRP/-LEU (control), -TRP/-LEU/-HIS (histidine) (low stringency), and -TRP/-LEU/-HIS/-ADE (adenine) (high stringency), grown for 2–3 days, then examined for growth.

For yeast three-hybrid assays, pBridge vectors containing either Spo16 or Zip2 in MCS I were further modified

by NotI cleavage at the MCS II site followed by isothermal assembly-mediated insertion of the second gene (58), resulting in a single vector encoding a Zip2:Spo16 complex containing the Gal4-BD tag fused to the N-terminus of either protein. These vectors were transformed into AH109 and mated with pGADT7 AD vectors encoding Zip4.

Protein expression and purification

Ligation-independent cloning was used to clone full length Spo16 and Zip2$^{499–704}$. To express TEV protease-cleavable, His_6-tagged Spo16, full-length Spo16 was cloned into Addgene vector 48324 (contains Spectinomycin resistance and CloDF13 ori) using ligation-independent cloning. To express untagged Zip2 499–704, DNA encoding Zip2 499–704 was cloned into Addgene vector 29665 (contains Ampicillin resistance and ColE1 origin of replication) using ligation-independent cloning. The Zip2 surface entropy reduction (SER) mutant (KEK 641–643 → AAA) was identified by the UCLA SERp server (http://services.mbi.ucla.edu/SER/) (59) and was generated by mutagenic PCR.

For protein expression, plasmids encoding Zip2$^{499–704}$ (unmutated or SER mutant) and full-length Spo16 were co-transformed into *E. coli* Rosetta2 (DE3) pLysS cells, and grown in 2XYT media supplemented with both ampicillin and spectinomycin. Cells were grown at 37°C to an OD_{600} of 0.6, shifted to 20°C and protein expression induced with 0.25 mM IPTG, and grown 16 hours. For selenomethionine derivatization, cells were grown in M9 minimal media at 37°C to an OD_{600} of 0.8, after which the following amino acids were added: Leu, Ile and Val (50 mg/l), Phe, Lys, Thr (100 mg/L) and Selenomethionine (60 mg/L). Cells were shifted to 20°C and protein expression was induced with 0.25 mM IPTG after 20 min incubation with amino acids.

For protein purification, cells were harvested by centrifugation, suspended in resuspension buffer (20 mM Tris–HCl pH 8.0, 300 mM NaCl, 10 mM imidazole, 1 mM dithiothreitol (DTT) and 10% glycerol) and lysed by sonication. Lysate was clarified by centrifugation (16 000 rpm 30 min), then supernatant was loaded onto a Ni^{2+} affinity column (HisTrap HP, GE Life Sciences) pre-equilibrated with resuspension buffer. The column was washed with buffer containing 20 mM imidazole and 100 mM NaCl, and eluted with a buffer containing 250 mM imidazole and 100 mM NaCl. The elution was loaded onto an anion-exchange column (Hitrap Q HP, GE Life Sciences) and eluted using a 100–600 mM NaCl gradient. Fractions containing the protein were pooled and concentrated to 2 ml by ultrafiltration (Amicon Ultra-15, EMD Millipore), then passed over a size exclusion column (HiLoad Superdex 200 PG, GE Life Sciences) in a buffer containing 20 mM Tris–HCl pH 8.0, 200 mM NaCl, and 1 mM DTT. The N-terminal His_6-tag on Zip2, while cleavable by TEV protease, was not removed for any experiments shown. Purified proteins were concentrated by ultrafiltration and stored at 4°C for crystallization, or aliquoted and frozen at −80°C for biochemical assays. All mutant proteins were purified as wild-type (Supplementary Figure S8).

Note regarding Zip2:Spo16 constructs. De Muyt *et al*. (55) recently reported DNA binding results using reconstituted Zip2(XPF domain):Spo16 complex that is similar, but not identical, to the complex used in this study. While both studies used the same Zip2 truncation (residues 499–704) and full-length Spo16, our construct used an N-terminal TEV protease-cleavable His_6-tag on Spo16 (not cleaved for biochemical or structural analysis), while De Muyt *et al*. used a C-terminal His_6-tag on Zip2.

Surface lysine residues on the Zip2$^{499–704}$:His_6-Spo16 complex were dimethylated by mixing protein at 1 mg/ml with 20 mM freshly-prepared Dimethylamine Borane Complex and 40 mM formaldehyde, incubation at 4°C for one hour, then quenching by addition of 100 mM glycine (Supplementary Figure S3A). Alkylated proteins were concentrated and purified by size-exclusion chromatography as above.

For size exclusion chromatography coupled to multi-angle light scattering (SEC-MALS), 100 μL of Zip2$^{499–704}$:His_6-Spo16 at 2.0 mg/ml was injected onto a Superdex 200 Increase 10/300 GL column (GE Life Sciences) in a buffer containing 20 mM HEPES pH 7.5, 300 mM NaCl, 5% glycerol, and 1 mM DTT. Light scattering and refractive index profiles were collected by miniDAWN TREOS and Optilab T-rEX detectors (Wyatt Technology), respectively, and molecular weight was calculated using ASTRA v. 6 software (Wyatt Technology).

Protein crystallization

Form 1 crystals were obtained in hanging drops with surface-lysine methylated Zip2$^{499–704}$:His_6-Spo16 at 10 mg/ml in a buffer containing 20 mM Tris–HCl pH 7.5 and 200 mM NaCl. Protein was mixed 1:1 with well solution containing 1.4 M Na–K phosphate pH 6.6. Crystals were transferred to a cryoprotectant solution containing 2.4 M Na malonate pH 7.0, then flash-frozen in liquid nitrogen. Form 2 crystals were obtained in hanging drops with Zip2$^{499–704}$SER:His_6-Spo16 at 10 mg/ml in a buffer containing 20 mM Tris–HCl pH 7.5 and 200 mM NaCl. Protein was mixed 1:1 with well solution containing 100 mM Bis Tris pH 5.5, 200 mM Ammonium sulfate, 15% PEG 3350. Crystals were cryo-protected by addition of 15–20% PEG 400, then flash-frozen in liquid nitrogen.

X-Ray data collection and structure determination

For Form 1, diffraction data was collected at the Advanced Photon Source, NE-CAT beamline 24ID-E (support statement below). Data was automatically indexed and reduced by the RAPD data-processing pipeline (https://github.com/RAPD/RAPD), which uses XDS (60) for indexing and integration, and the CCP4 programs AIMLESS and TRUNCATE (61) for scaling and structure-factor calculation. Extensive efforts to determine the structure by anomalous methods using selenomethionine-derivatized protein failed due to translational pseudo-symmetry arising from the positions and orientations of the four copies of Zip2$^{499–704}$:Spo16 in these crystals.

For Form 2, diffraction data for both native and selenomethionine-derivatized crystals were collected at the Advanced Photon Source, NE-CAT beamline 24ID-C, and data was automatically indexed and reduced by RAPD.

The structure was determined by single-wavelength anomalous diffraction (SAD) methods using a 2.38 Å-resolution dataset collected from selenomethionine-derivatized proteins. Selenium sites were located using hkl2map/SHELX (62,63), and provided to the Phenix Autosol pipeline (64,65) for phase calculation using PHASER (66) and density modification using RESOLVE (67). A partial model built by RESOLVE (68) was manually rebuilt in COOT (69) and refined against a 2.13 Å-resolution native dataset using phenix.refine (70).

To determine the Form 1 structure, molecular replacement was performed using PHASER to place four copies of the Form 1 dimer structure. The model was manually rebuilt in COOT and refined in phenix.refine to 2.29 Å resolution. Refined electron-density maps revealed several ordered dimethyllysine side-chains (Supplementary Figure S3B) and additional electron density extending the side-chain of Zip2 Cys521 in all four copies of the complex. Formaldehyde, which was used for surface lysine alkylation of the complex, can react with the cysteine side-chain to produce hydroxymethylcysteine (71,72), which closely matches the observed electron density for this residue (Supplementary Figure S3C, D). We also observed clear electron density for several residues in the N-terminal His_6-tag fused to Spo16, which included a TEV protease cleavage site (MKSSHHHHHHENLYFQ^SNA-[$Spo16^{2–198}$]), packing against a symmetry-related copy of Spo16, explaining why these crystals required an intact tag for growth (Supplementary Figure S3E). Data collection and refinement statistics for both structures can be found in Supplementary Table S1. All structure figures were created with PyMOL version 2, and surface charge calculations were performed with the APBS (73) plugin in PyMOL. Original diffraction data have been deposited with the SBGrid Data Bank (https://data.sbgrid.org) under accession numbers 538 ($Zip2^{499–704}$:Spo16 Form 1 Native), 539 ($Zip2^{499–704}$SER:Spo16 Form 2 Native), and 540 ($Zip2^{499–704}$SER:Spo16 Form 2, selenomethionine-derivatized SAD dataset). Reduced data and refined structures have been deposited with the RCSB Protein Data Bank (https://www.rcsb.org) under accession numbers 6BZF ($Zip2^{499–704}$:Spo16 Form 1) and 6BZG ($Zip2^{499–704}$SER:Spo16 Form 2).

APS NE-CAT support statement. This work is based upon research conducted at the Northeastern Collaborative Access Team beamlines, which are funded by the National Institute of General Medical Sciences from the National Institutes of Health (P41 GM103403). The Pilatus 6M detector on 24-ID-C beam line is funded by a NIH-ORIP HEI grant (S10 RR029205). This research used resources of the Advanced Photon Source, a U.S. Department of Energy (DOE) Office of Science User Facility operated for the DOE Office of Science by Argonne National Laboratory under Contract No. DE-AC02-06CH11357.

DNA binding assays

To generate different DNA substrates for electrophoretic mobility shift assays, a 40-base oligonucleotide 5′-labeled with 6-carboxyfluorescein (5′-6-FAM_40bp) was annealed at 10 μM concentration in annealing buffer (10 mM Tris–HCl pH 8.0, 50 mM NaCl, 1 mM $MgCl_2$, 1 mM EDTA) with specific unlabeled oligos (sequences in Supplementary Table S2) as follows: ssDNA (5′-6-FAM_40bp alone); dsDNA (5′-6-FAM_40 bp + 40 bp_for_ds); 5′-overhang (5′-6-FAM_40 bp + 20 bp_for_free5′); 3′-overhang (5′-6-FAM_40 bp + 20 bp_for_free3′); HJ (5′-6-FAM_40 bp + HJ_strand2 + HJ_strand3 + HJ_strand4). Annealing was performed in a PCR machine using a temperature gradient from 95°C to 4°C, at a speed of 0.1°C/s. EMSA reactions were prepared (buffer contained 20 mM Tris–HCl pH 8.0, 1 mM DTT, 5 mM $MgCl_2$, 5% glycerol) by keeping the DNA concentration constant at ∼55 nM and varying the protein concentration. After 10 min incubation and addition of 5% (w/v) sucrose, free DNA and DNA-protein complexes were resolved by electrophoresis on 6% TBE-acrylamide gels pre-equilibrated (pre-run for 30 min at 150 V) in 0.2X TBE running buffer. Gels were run for 40 min at 100V at 4°C. Gels were imaged using a Bio-Rad ChemiDoc system using filters to image Cy2 dye. Gel bands were quantified using ImageJ (https://imagej.net), and binding curves were calculated using GraphPad Prism (https://www.graphpad.com) using a single-site binding model:

$$Y = \frac{B_{max} \times X}{K_d + X}$$

where Y is fraction of DNA bound, X is protein concentration, B_{max} is maximum possible DNA bound (constrained to 1), and K_d is the dissociation constant.

Isothermal titration calorimetry was performed on a Microcal ITC 200 (Malvern Panalytical) in a buffer containing 20 mM Tris (pH 8.5), 300 mM NaCl, and 1 mM TCEP. $Zip2^{499–704}$:Spo16 at 230 μM was injected into an analysis cell containing 20 or 25 μM DNA.

RESULTS

Architecture of the Zip2:Zip4:Spo16 complex

Zip2, Zip4, and Spo16 share similar roles in promoting meiotic crossover formation and synaptonemal complex assembly, co-localize on meiotic chromosomes, and depend on one another for their chromosome localization (48,49). Recently, De Muyt *et al.* showed that the three proteins can be co-purified from meiotic cell lysate, directly interact in yeast two-hybrid assays, and depend on one another for localization to DNA double-strand breaks sites (55). To complement this work and comprehensively outline interactions between Zip2, Spo16 and Zip4, we first used yeast two-hybrid analysis. We found that Spo16 binds the conserved C-terminal region of Zip2 (residues 499–704), which contains Zip2′s predicted XPF-like domain (Figure 1A,B). We also found that full-length Zip2 and the isolated Zip2 N-terminal region (residues 1–499) interact with full-length Zip4, though we detected these interactions with only one tag configuration (Figure 1B, Supplementary Figure S1A). We did not detect a direct interaction between Spo16 and Zip4, which was previously reported by De Muyt *et al.* (55). We next attempted to identify the Zip4-binding region of Zip2 by progressively truncating the Zip2 N-terminus. For these experiments, we used a yeast three-hybrid assay with

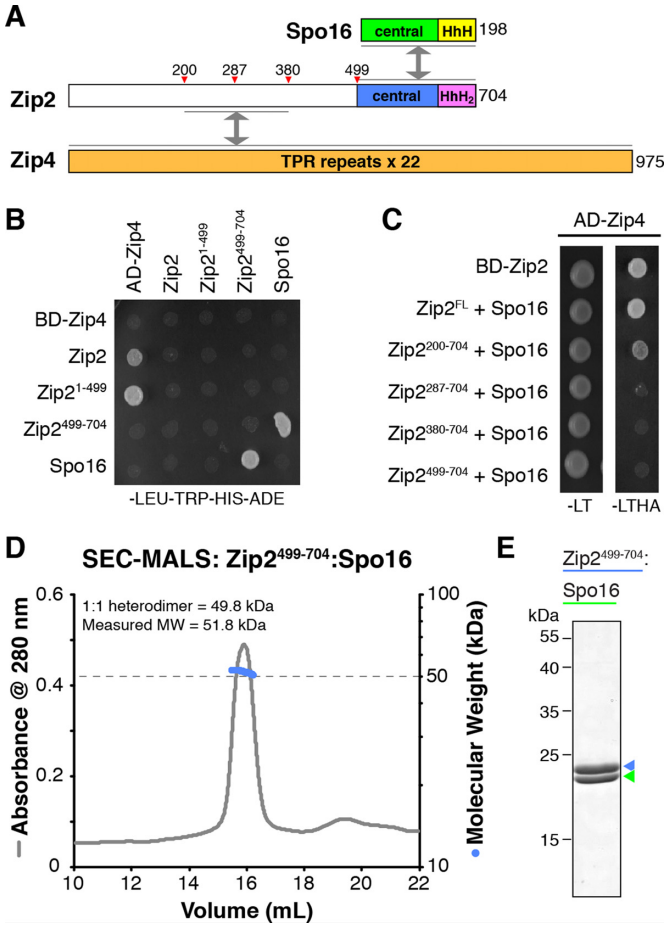

Figure 1. Zip2, Zip4, and Spo16 form a complex. (**A**) Domain structure of Zip2, Zip4, and Spo16. Gray arrows indicate interactions identified by yeast two-hybrid and yeast three-hybrid analysis. The N-terminal domain of Zip2 has been proposed to contain a WD40 β-propeller domain (36), but the region is poorly conserved (Supplementary Figure S2) and modern structure-prediction algorithms do not support this assignment. HhH: helix-hairpin-helix, HhH_2: tandem helix-hairpin-helix. (**B**) Yeast two-hybrid analysis of interactions between Zip2, Zip4, and Spo16. See Supplementary Figure S1A for complete results. (**C**) Yeast three-hybrid analysis. See Supplementary Figure S1B for complete results. (**D**) Size exclusion chromatography/multi-angle light scattering (SEC-MALS) analysis of purified $Zip2^{499–704}$:Spo16. The measured molecular weight (51.8 kDa) is consistent with a 1:1 heterodimer (molecular weight 49.8 kDa). (**E**) SDS-PAGE analysis of purified $Zip2^{499–704}$:Spo16.

one vector encoding both Zip2 and Spo16 in order to stabilize Zip2 in solution, and a second vector encoding Zip4. We detected a strong interaction in this assay that was dependent on the N-terminal region of Zip2 (Figure 1C, Supplementary Figure S1B). Truncation of the N-terminal 200 residues of Zip2 did not affect Zip4 binding, while removal of 380 residues completely disrupted binding. An intermediate truncation of 287 residues resulted in a near-complete loss of detectable binding under stringent selection (media lacking leucine/tryptophan/histidine/adenine; Figure 1C), but showed self-activation under less stringent selection (media lacking leucine/tryptophan/histidine; Supplementary Figure S1B), complicating interpretation of this construct. While the N-terminal region of Zip2 is mostly poorly conserved, the region spanning residues 200–380 does contain several short, highly-conserved motifs, one or more of which may be responsible for Zip4 binding (Supplementary Figure S2). Together, these data strongly indicate that Zip2 is the key central component of the Zip2:Zip4:Spo16 complex, with its N-terminal domain binding Zip4 and its C-terminal domain binding Spo16. Efforts to identify the Zip2-binding region of Zip4 by deletion analysis were unsuccessful, likely due to structural disruption when truncating Zip4′s predicted array of TPR repeats (not shown).

The Zip2:Spo16 structure reveals an XPF:ERCC1-like complex

We next co-expressed Zip2 and Spo16 in *E. coli* for structural and biochemical analysis. While full-length Zip2 expressed poorly and was mostly insoluble, even when co-expressed with Spo16, we could co-express and purify the Zip2 XPF-like region (residues 499–704) with Spo16. The $Zip2^{499–704}$:Spo16 complex forms a well-behaved 1:1 heterodimer, as measured by size exclusion chromatography coupled to multi-angle light scattering (SEC-MALS; Figure 1D, E). While initial crystallization efforts were unsuccessful, we obtained crystals of the complex after chemical methylation of surface lysine residues (Methods; Supplementary Figure S3A-D) (74,75). The resulting crystals (termed Form 1 hereon) adopted space group C2 and contained four copies of the complex per asymmetric unit. Extensive efforts to determine the structure of Form 1 crystals using heavy-atom derivatives failed due to translational pseudo-symmetry in these crystals.

To identify additional crystal forms for the $Zip2^{499–704}$:Spo16 complex, we turned to surface entropy reduction, a strategy to promote crystallization by mutating short stretches of large polar residues to alanine (76). We mutated the highest-scoring segment in Zip2 identified by the UCLA SERp Server (59), residues 641–643, from the sequence KEK to AAA (Supplementary Figure S2). The mutated complex, $Zip2^{499–704}$SER:Spo16, behaved equivalently to wild-type protein *in vitro* but crystallized in several new conditions without surface lysine methylation. We optimized one condition in space group $P2_12_12_1$ (termed Form 2 hereon), which contained one copy of the $Zip2^{499–704}$SER:Spo16 complex per asymmetric unit, and determined the structure by single-wavelength anomalous diffraction methods (Figure 2A, Supplementary Table S1). We then used molecular replacement to determine the Form 1 structure, yielding a total of five crystallographically-independent views of the $Zip2^{499–704}$:Spo16 complex. These five structures are nearly identical (overall Cα r.m.s.d. 0.3–1.4 Å; Supplementary Figure S3F), indicating that neither crystallization strategy—surface lysine methylation nor surface entropy reduction—significantly alters the complex's structure.

The overall structure of $Zip2^{499–704}$:Spo16 is similar to known XPF:ERCC1 and related complexes (Figure 2A, B). Zip2 possesses an XPF-like central domain (residues 499–640) and a C-terminal tandem helix-hairpin-helix (HhH_2) domain (residues 641–704) (Figure 2B–E). Spo16 shows a similar two-domain structure, with an N-terminal central domain similar in fold to ERCC1, though significantly diverged (Figure 2B–D). As XPF and ERCC1 are descended

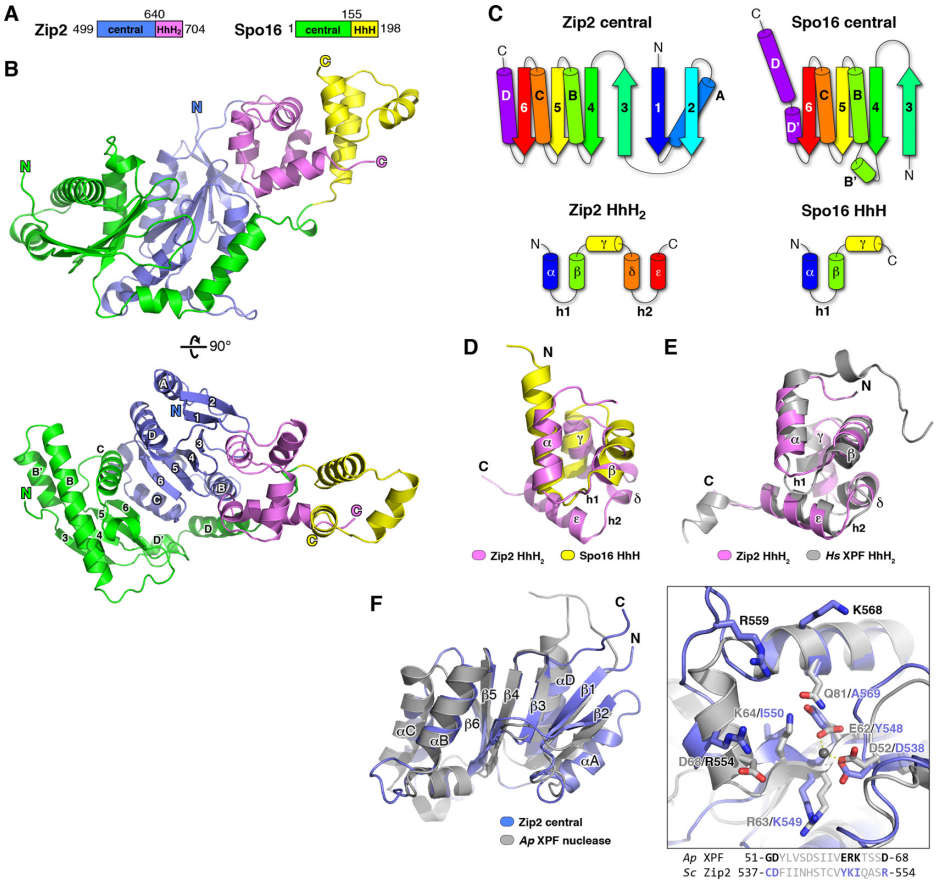

Figure 2. Structure of the Zip2$^{499–704}$:Spo16 complex. (**A**) Domain schematic of Zip2 (truncated construct for crystallization) and Spo16. (**B**) Two views of the Zip2$^{499–704}$:Spo16 dimer, with domains colored as in (A). In one view, secondary structure elements of both proteins' central domains are labeled as in panel (C). See Supplementary Figure S3F for an overlay of the five crystallographically-independent views of the dimer. (**C**) Secondary structure of the Zip2 and Spo16 central domains (top) and HhH domains (bottom). (**D**) Overlay of the Zip2 HhH_2 and Spo16 HhH domains. Cα r.m.s.d. = 2.65 Å over 34 atom pairs. HhH #1 comprises helices α and β separated by hairpin 1 (h1), and HhH #2 (not shared by Spo16) comprises helices δ and ε, separated by hairpin 2(h2). (**E**) Overlay of the Zip2 HhH_2 domain (pink) with the HhH_2 domain of *H. sapiens* XPF (PDB ID 1Z00; gray). Cα r.m.s.d. = 1.97 Å over 51 atom pairs. (F) Overlay of the Zip2 central domain (blue) with the *Aeropyrum pernix* XPF nuclease domain (gray) (PDB ID 2BGW) (79). Cα r.m.s.d. = 2.50 Å over 107 atom pairs. *Left:* close-up of the active site of *A. pernix* XPF (gray, with bound Mg^{2+} ion shown as a sphere) with the equivalent region of the Zip2 central domain (blue). Zip2's DNA binding patch 1 (see Figure 4B) comprises residues R554, R559 and K568 (labeled in black).

from a common ancestor and possess similar overall folds (77), so too do Zip2 and Spo16 share a common overall architecture. As previously predicted by De Muyt *et al.* (55), the Spo16 C-terminal domain contains only a single HhH motif as opposed to the tandem HhH motifs found in ERCC1 (Figure 2C,D). The Zip2 and Spo16 central domains form a tight pseudo-symmetric dimer, with flexible linkers connecting these domains to the C-terminal HhH domains, which also form a tight dimer. The conformations of the linker regions and the relative positions of the central and HhH domains are identical in the five independent views of the Zip2$^{499–704}$:Spo16 complex (Supplementary Figure S3F), suggesting that the complex is relatively rigid, at least in the absence of DNA (see below). The juxtaposition of central and HhH domains is also similar to a recent structure of the human FANCM:FAAP24 complex, an inactive XPF:ERCC1-like complex with a key role in scaffolding the Fanconi Anemia 'core' DNA-repair complex (57).

The key biochemical activities of XPF:ERCC1 are structure-specific DNA binding and single-strand DNA cleavage, primarily at single-strand—double-strand DNA junctions, as part of its role in the nucleotide excision repair pathway (78). DNA cleavage is catalyzed at a highly-conserved active site on the XPF central/nuclease domain. Prior sequence analyses of Zip2 and both *A. thaliana* and mammalian SHOC1 have suggested that these proteins likely lack endonuclease activity (53–55), and Zip2 was shown to lack endonuclease activity in vitro on a typical XPF:ERCC1 substrate (55). We overlaid the Zip2 central domain with the structure of *Aeropyrum pernix* XPF nuclease domain (79), and examined the region around the putative active site (Figure 2F). XPF-family proteins possess a highly-conserved motif, GDx_nERKx_3D, which contains residues responsible for Mg^{2+} ion binding and DNA cleavage (80). Of the highly-conserved residues in the XPF active-site motif, Zip2 possesses only one, D538, which corresponds to the first aspartate in the conserved XPF motif (D52 in *A. pernix* XPF; Figure 2F, Supplementary Figure S2). The region of Zip2 corresponding to the $ERKx_3D$ motif of XPF proteins does not contain any of these residues, and is highly variable across fungal Zip2 orthologs (Fig-

ure 2F, Supplementary Figure S2). Further, when we determined a structure from crystals grown in the presence of 10 mM $MgCl_2$, we saw no evidence of a bound Mg^{2+} ion in this site (not shown). Thus, despite the conservation of one key active site residue with XPF, our structural evidence overall points to Zip2 lacking endonuclease activity, in agreement with prior biochemical analysis (55) and our own data (see below). This finding is again reminiscent of the FANCM:FAAP24 complex, in which the XPF ortholog FANCM also lacks endonuclease activity. Since FANCM:FAAP24 is thought to bind specific DNA structures and scaffold the assembly of a multi-subunit DNA repair complex (57), a similar DNA binding/scaffolding activity could explain existing genetic data on the roles of *ZIP2* and *SPO16* in CO formation.

Zip2:Spo16 binds a range of DNA structures

The structural similarity of Zip2$^{499–704}$:Spo16 to XPF:ERCC1 and related complexes including FANCM:FAAP24 and Mus81:Eme1 strongly suggests a structure-specific DNA binding function for this complex. Further, the delay in formation of single-end invasion and double Holliday Junction intermediates in *spo16* mutants (49) suggests that the complex may bind and stabilize a specific recombination intermediate to promote crossover formation. To test for DNA binding activity, we performed quantitative electrophoretic mobility-shift assays (EMSA) with reconstituted Zip2$^{499–704}$:Spo16 and DNA substrates containing structural elements found in meiotic recombination intermediates. We first tested binding of Zip2$^{499–704}$:Spo16 to a 40-base single-stranded DNA (ssDNA) and a 40-base pair double-stranded DNA duplex (dsDNA). In agreement with the earlier findings of De Muyt *et al.* (55), Zip2$^{499–704}$:Spo16 bound robustly to dsDNA (K_d = 14 μM; Figure 3A) but did not detectably interact with ssDNA (not shown). We next tested binding to ssDNA–dsDNA junctions, as XPF:ERCC1 family complexes recognize these structures for cleavage, and because strand invasion during meiotic homologous recombination generates a D-loop intermediate that features a ssDNA–dsDNA junction with a 5′ overhang. We found that Zip2$^{499–704}$:Spo16 binds both 5′-overhang and 3′-overhang junction DNA with an affinity roughly equivalent to its affinity for dsDNA (5′ overhang K_d = 9 μM, 3′ overhang K_d = 17 μM; Figure 3B, C), suggesting that the complex may not specifically recognize ssDNA–dsDNA junctions. We next tested binding to a 40-bp dsDNA with a nick centrally-located in one strand, and measured a K_d of 6 μM (Figure 3D). The 2-fold tighter K_d for nicked versus un-nicked dsDNA suggests that Zip2$^{499–704}$:Spo16 may preferentially bind highly bent or bendable DNA.

We next tested binding of Zip2$^{499–704}$:Spo16 to Holliday Junction (HJ) DNA and a variant HJ with one nicked strand (nicked HJ). A recent study of heteroduplex DNA generated during *S. cerevisiae* meiotic recombination revealed a strong bias in the pattern of dHJ resolution toward cleavage of the newly-synthesized strands (81). This finding suggested that COs may be generated by Mlh1:Mlh3-mediated cleavage of an unligated dHJ containing nicks on these newly-synthesized strands. Given the involvement of

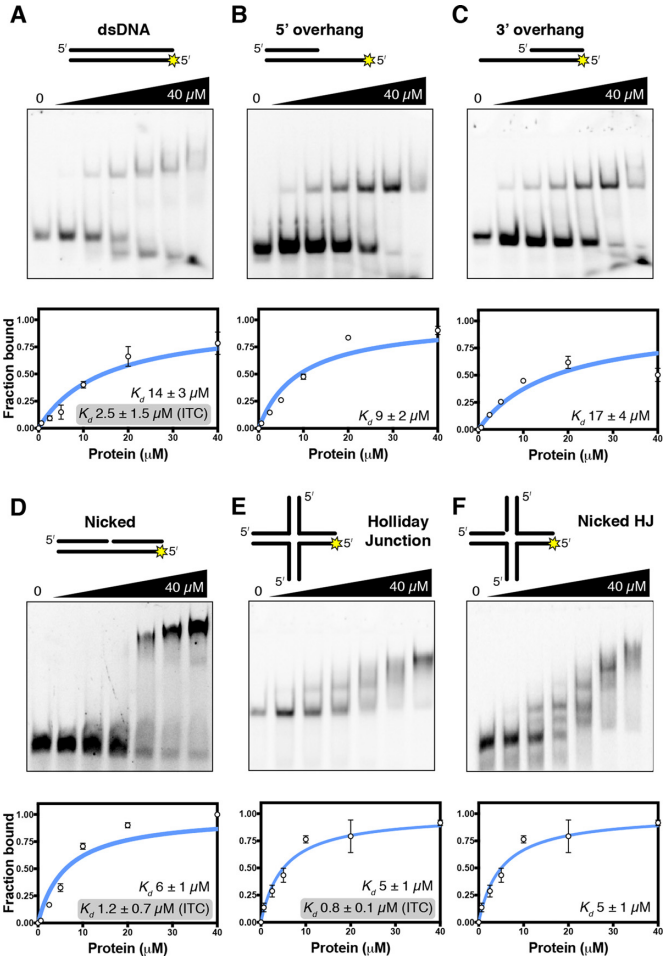

Figure 3. DNA binding by Zip2$^{499–704}$:Spo16. Representative gel-shift (*upper*) and binding curve from triplicate experiments (*lower*) for Zip2$^{499–704}$:Spo16 binding dsDNA (**A**), 5′-overhang (**B**), 3′-overhang (**C**), nicked (**D**), Holliday Junction (**E**), and nicked Holliday Junction (**F**) DNA substrates. Protein concentrations in each lane (left to right: 0, 0.625, 2.5, 5, 10, 20, and 40 μM) are the same for all gels. Red asterisks indicate location of multiple shifted bands for the HJ substrate. Gray boxes indicate K_d values for dsDNA, nicked DNA, and Holliday Junction DNA as measured by isothermal titration calorimetry (Supplementary Figure S4).

Zip2, Zip4 and Spo16 in CO formation, one possibility for their action may be to recognize the nicked strand in an unligated HJ, and direct Mlh1:Mlh3 activity to the opposite strand (see Discussion). We observed robust binding of Zip2$^{499–704}$:Spo16 to both HJ substrates, comparable to the nicked dsDNA substrate (K_d = 5 μM for both HJ and nicked HJ; Figure 3E, F). We also observed multiple shifted bands on our gels with both HJ substrates, suggesting that multiple Zip2$^{499–704}$:Spo16 complexes may bind a single HJ at high protein concentrations. We did not observe a preference for nicked over fully-ligated HJ substrates, suggesting that at least on its own, Zip2$^{499–704}$:Spo16 is unable to specifically recognize the nicked strand in an unligated HJ.

We next used isothermal titration calorimetry (ITC) to verify binding of Zip2$^{499–704}$:Spo16 to several DNA substrates. We measured a binding affinity of 2.5 μM for Zip2$^{499–704}$:Spo16 binding dsDNA (Supplementary Figure S4A), roughly 5-fold tighter than the affinity we measured

by EMSA (14 μM). We next measured binding affinities of ∼1 μM for Zip2$^{499–704}$:Spo16 binding both nicked DNA (Supplementary Figure S4B) and HJ DNA (Supplementary Figure S4C); as with dsDNA, these affinities are roughly 5-fold tighter than those measured by EMSA (5–6 μM). Due to low signal-to-noise in ITC experiments, we were unable to measure binding of Zip2$^{499–704}$:Spo16 to either nicked HJ or ssDNA–dsDNA junction substrates by ITC (not shown). Nonetheless, these ITC data confirm that Zip2$^{499–704}$:Spo16 preferentially binds nicked and HJ DNAs over dsDNA, supporting the idea that the complex recognizes junctions or bent/bendable DNA segments. Finally, our ITC data also revealed very slow equilibration kinetics and a large positive entropy change (ΔS) upon binding to all substrates (Supplementary Figure S4C), suggesting that Zip2$^{499–704}$:Spo16 may undergo a significant conformational change upon DNA binding.

As noted above, prior sequence analysis (55) and our structures have suggested that unlike XPF, Zip2 does not possess nuclease activity. To test for nuclease activity directly, we incubated Zip2$^{499–704}$:Spo16 at 30°C with three different labeled DNA substrates, then analyzed the results by denaturing urea-PAGE (Supplementary Figure S5). We observed no evidence for nuclease activity, in agreement with both our sequence/structure analysis and prior biochemical analysis by De Muyt *et al*. (55).

Overall, our biochemical analysis shows that Zip2$^{499–704}$:Spo16 robustly binds multiple DNA structures that likely exist in early meiotic recombination intermediates, including branched structures and ssDNA–dsDNA junctions. While the complex does not show strong structure-specific binding, preferential binding of nicked and HJ DNA in particular suggests that the complex may recognize a bent or branched structure, and may even participate directly in dictating dHJ cleavage geometry (see Discussion). Our data largely mirror recent findings by De Muyt *et al*., who found that a reconstituted Zip2(XPF domain):Spo16 complex binds branched DNA structures with subtly higher affinity than dsDNA (55). Interestingly, De Muyt *et al*. identified a D-loop as the most-preferred substrate, but given the complexity of this substrate, which includes both ssDNA–dsDNA junctions and branched structures, it is unclear which element in this substrate is specifically recognized by Zip2:Spo16 (55). Similarly, Guiraldelli *et al*. recently showed that purified mammalian SHOC1 binds both D-loop and Holliday Junction structures more tightly than dsDNA, though these assays also included an N-terminal SHOC1 domain predicted to adopt a helicase fold, and did not include an ERCC1-like binding partner (54).

To identify likely DNA-binding surfaces on Zip2$^{499–704}$:Spo16, we examined known DNA co-crystal structures of related enzymes. The *Aeropyrum pernix* XPF homodimer has been co-crystallized with double-stranded DNA (79), and the isolated HhH_2 domain of human XPF has been co-crystallized with single-stranded DNA (82). In addition, human MUS81:EME1 has been co-crystallized with several more complex DNAs including 5′ and 3′ flap structures (83). The MUS81:EME1-DNA structures are particularly informative, as they show how these proteins' central/nuclease and HhH_2 domains cooperate to bind a single DNA substrate and orient it for cleavage. To model the DNA-bound conformation of Zip2$^{499–704}$:Spo16, we used a structure of MUS81:EME1 bound to a 5′-flap DNA substrate, which (as the 5′-flap itself is disordered in the structure) closely mimics the nicked DNA substrate that Zip2$^{499–704}$:Spo16 preferentially binds (Supplementary Figure S6). The DNA is bent nearly 90° about the broken DNA strand in the MUS81:EME1-DNA complex, in agreement with our speculation that bent or highly bendable structures (which would also include branched structures like Holliday Junctions) are preferred substrates of Zip2$^{499–704}$:Spo16. In this structure, the central and HhH_2 domains of MUS81:EME1 are separated, sandwiching the DNA substrate between them (83). While Zip2$^{499–704}$:Spo16 shows a consistent overall structure in all five crystallographic views of the complex, closer inspection of the interface between the central and HhH_2/HhH regions reveals that it is relatively small and mostly hydrophilic (not shown). Further, the inter-domain linkers on both Zip2 and Spo16 are long enough to allow significant conformational changes, and our ITC data suggested that the complex may undergo a conformational change upon binding DNA (Supplementary Figure S4C). Thus, we separately overlaid the central and HhH domains of Zip2$^{499–704}$:Spo16 onto the structure of MUS81:EME1. The resulting model shows a significant conformational shift of the HhH domains relative to their orientation in our crystal structures, but the two regions remain close enough that the inter-domain linkers in each protein can easily span the distance (Figure 4A). Based on this model, sequence alignments, and known DNA-binding surfaces of XPF-family proteins, we identified four surfaces on the Zip2$^{499–704}$:Spo16 complex that are potentially involved in binding DNA (Supplementary Figure S7). Patch 1, located on the Zip2 central domain, is close to the active site in related XPF-family proteins, and comprises three positively-charged residues: R554, R559 and K568 (Figures 2E, 4B). Patch 2 borders patch 1, and includes residue K600 of Zip2 and two Spo16 residues, R127 and N132 (Figure 4B). Both patches 1 and 2 are juxtaposed to DNA in our model. Patches 3 and 4 are located on adjacent surfaces of the Zip2 HhH_2 domain, with patch 3 comprising residues K663, K683, and K686, and patch 4 comprising residues N657, Q692, and R695 (Figure 4C). Patch 3 is equivalent to a surface on human XPF previously shown to bind single-stranded DNA (82), while patch 4 corresponds to the surface on MUS81 that interacts with double-stranded DNA (83).

To test the roles of the four putative DNA-binding surfaces on Zip2$^{499–704}$:Spo16, we mutated these surfaces and tested binding of both 5′ overhang and nicked DNA substrates by EMSA. We found that mutants in patches 1, 2 and 3 do not affect complex formation (Supplementary Figure S8) but strongly affect binding to both DNA substrates (Figure 4D-F, Supplementary Figure S9), supporting our model of DNA binding by Zip2$^{499–704}$:Spo16. Further, these results show that both the central and HhH domains, acting together, are required for robust DNA binding. We were unable to purify complexes containing mutants in patch 4, potentially because these residues are involved in inter-domain contacts in the non-DNA-bound

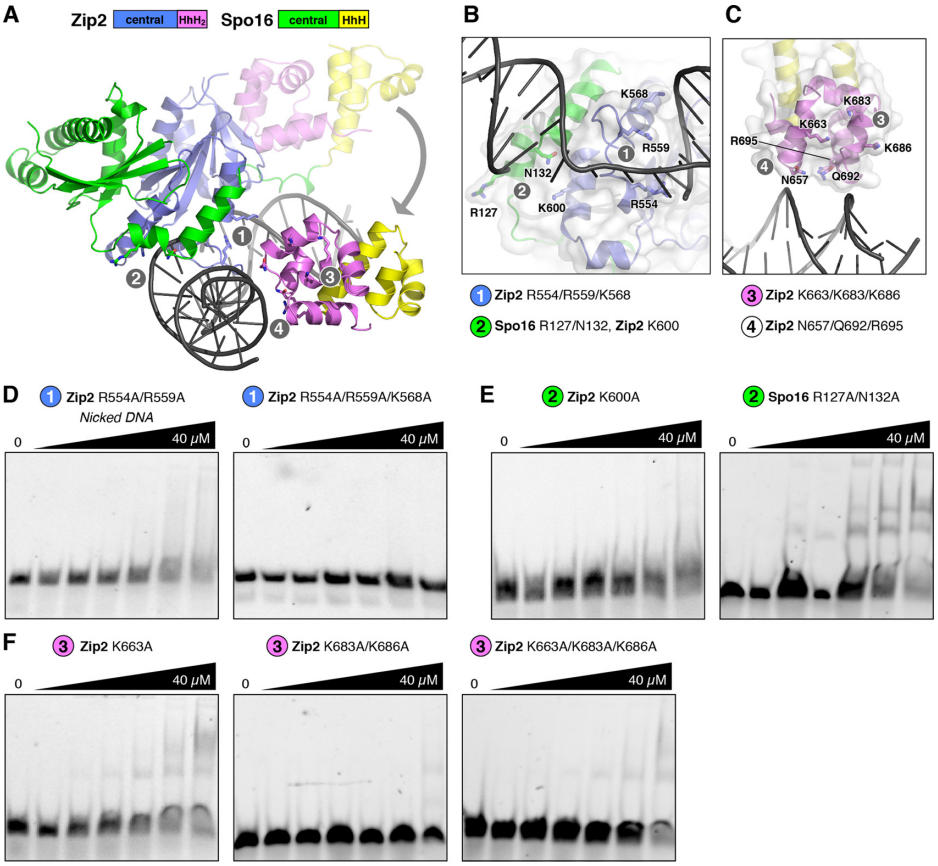

Figure 4. Identification of DNA-binding surfaces of Zip2$^{499–704}$:Spo16. (A) Model of the Zip2$^{499–704}$:Spo16 complex bound to a nicked/overhang DNA, based on a structure of human Mus81:Eme1 in complex with a 5′-flap DNA (PDB ID 4P0R (83); see Supplementary Figure S6). The central domains are oriented equivalently to Figure 2A. In the model, the HhH domains of Zip2 and Spo16 have undergone a significant conformational change from their original orientation (semi-transparent ribbons) upon DNA binding (gray arrow). Gray circles indicate the locations of putative DNA-binding patches 1–4. See Supplementary Figure S7 for surface charge distribution. (**B**) Close-up view of patches 1 and 2 on the central domains of Zip2 and Spo16. See Supplementary Figure S7B for surface charge distribution. (**C**) Close-up view of patches 3 and 4 on the Zip2 HhH_2 domain. See Supplementary Figure S7C for surface charge distribution. (**D**) Representative gel-shift assays for patch 1 mutants binding nicked DNA. See Supplementary Figure S9 for binding of 5′ overhang DNA and HJ DNA by these mutants. (**E**) Representative gel-shift assays for patch 2 mutants binding nicked DNA. (**F**) Representative gel-shift assays for patch 3 mutants binding nicked DNA.

structure of Zip2$^{499–704}$:Spo16 (not shown). We were therefore unable to test the role of patch 4 in DNA binding.

DISCUSSION

The data we present here shows that the *S. cerevisiae* Zip2:Spo16 complex forms an XPF:ERCC1-like dimer with a preference for binding bent/bendable or branched DNA structures. We further show that the Zip2 N-terminal domain binds Zip4, likely scaffolding the assembly of a larger Zip2:Zip4:Spo16 complex. Based on prior work, the Zip2:Zip4:Spo16 complex is required for formation of type 1 interfering COs in yeast, and also is required for polymerization of the synaptonemal complex in coordination with crossover formation. Based on its structure and DNA binding activity, we propose that Zip2:Spo16 binds a specific DNA structure generated early in the recombination pathway, thereby promoting resolution of this intermediate as a type I CO (Figure 5). Zip2:Spo16 could bind an element of the initial D-loop intermediate, cooperating with Msh4:Msh5 to stabilize this intermediate against dissolution by topoisomerases/helicases. Supporting this idea, recent work by De Muyt *et al.* (55) showed that in vitro, Zip2:Spo16 binds a D-loop with high affinity. A second possibility is that Zip2:Spo16 specifically binds the Holliday Junctions generated later in the recombination pathway, perhaps recognizing the nicked strands in an unligated dHJ intermediate and directing the nicking activity of the Mlh1:Mlh3 complex to the opposite strand to promote CO formation (Figure 5). This idea is supported by recent work showing a strong bias in the resolution pattern of dHJs in Mlh1:Mlh3-mediated CO formation in yeast (81), and parallels earlier proposals for biased resolution of unligated dHJs in other organisms (84).

In addition to promoting and stabilizing early recombination intermediates, Zip2:Zip4:Spo16 is also important for assembly of the synaptonemal complex, likely linking events at the DNA level with 'licensing' of synaptonemal complex assembly once recombination has progressed to a certain point. We propose that, similar to the role of FANCM:FAAP24 in the FA core complex, Zip2:Zip4:Spo16 can recruit and organize different proteins to promote the crossover fate and link crossover progres-

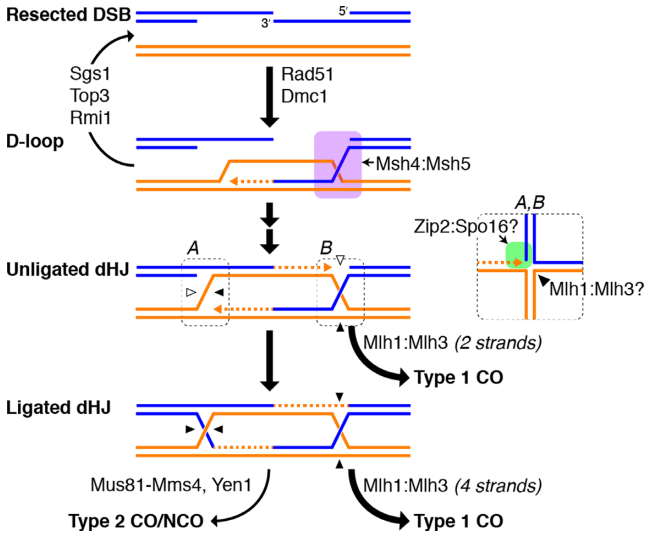

Figure 5. Model for the role of Zip2:Spo16:Zip4 in meiotic crossover formation. Model for the function of Zip2:Zip4:Spo16 in meiotic recombination. Initial strand invasion is mediated by Rad51 and Dmc1, and is continually counteracted by the dissolution activities of Sgs1, Top3 and Rmi1, resulting in SDSA. Recognition of specific DNA structures by Msh4:Msh5 (pro-HJ; pink shading) and Zip2: stabilize the strand-invasion/D-loop intermediate. Inset: Potential role of Zip2:Spo16 in recognizing unligated/nicked Holliday Junctions and directing the cleavage activity of Mlh1:Mlh3 to promote crossover formation. Additional protein complexes scaffolded by Zip4 may license assembly of the synaptonemal complex in coordination with crossover formation.

sion with chromosome axis remodeling and synaptonemal complex assembly. This recruitment is likely accomplished mostly by Zip4, which is predicted to fold into an array of 22 TPR repeats (36). Recently, De Muyt *et al.* identified a large number of potential interaction partners of the Zip2:Zip4:Spo16 complex using mass spectrometry, and demonstrated that Zip4 interacts directly with several of these, including the axis protein Red1 and the ZMM proteins Zip3 and Msh5 (55). These data support a model in which Zip2 and Spo16 recognize and stabilize a specific early recombination intermediate, while Zip4 is largely responsible for specific protein-protein interactions necessary for linking DNA recognition to downstream events including later stages of recombination and chromosome morphology changes.

In addition to protein interactions mediated by Zip4, close inspection of our Zip2$^{499–704}$:Spo16 complex reveals a conserved, concave hydrophobic surface involving the C-terminal W704 residue of Zip2 and two α-helices from the Spo16 HhH domain (Supplementary Figure S10). This interface binds a short hydrophobic α-helix on the Zip2 central domain in three of the five independent views of the complex (two of the four copies in Form 1, plus the single copy from Form 2), burying 410 Å^2 of mostly-hydrophobic surface area on each partner. Based on the high conservation of the involved residues on the Spo16 HhH domain, their mostly hydrophobic nature, and our observation of this interface in both crystal forms of Zip2$^{499–704}$:Spo16, we propose that this surface may be involved in specific protein-protein interactions. While our initial yeast two-hybrid assays revealed no interactions between Zip2:Spo16 and other known ZMM/chromosome axis/synaptonemal complex proteins (not shown), the role of this surface in protein-protein interactions will be an interesting avenue for future work, especially given the likelihood that Zip2:Zip4:Spo16 acts a scaffolding complex for DNA repair and synaptonemal complex assembly.

In *A. thaliana*, SHOC1 and PTD interact with one another and are required for the formation of type 1 COs, and sequence analyses have suggested that these proteins also form an XPF:ERCC1-like dimer (53,56). More recent work has shown that human SHOC1 localizes to meiotic recombination sites and is required for MLH1 localization and formation of chiasmata (54). When considered alongside the key roles of Zip2:Zip4:Spo16 in *S. cerevisiae* meiosis, these data strongly support the idea that an XPF:ERCC1-like DNA binding complex is an important and highly conserved feature of meiotic crossover control in eukaryotes. Further work will be required to identify Zip4-like scaffolding subunits in organisms outside fungi, and to determine how this conserved complex cooperates with Msh4:Msh5 to promote the crossover fate, and coordinate recombination with chromosome morphology changes such as chromosome axis remodeling and synaptonemal complex assembly.

DATA AVAILABILITY

Atomic coordinates and structure factors for the reported crystal structures have been deposited with the Protein Data Bank (http://www.pdb.org) under accession numbers 6BZF and 6BZG. Original diffraction data have been deposited at the SBGrid Data Bank (https://data.sbgrid.org) under accession numbers 538, 539, and 540.

SUPPLEMENTARY DATA

Supplementary Data are available at NAR Online.

ACKNOWLEDGEMENTS

The authors thank the staff of NE-CAT Sector 24 beamlines at the Advanced Photon Source for assistance with data collection, processing and phasing; A. Bobkov (Sanford Burnham Prebys Medical Discovery Institute, Protein Analysis Core Facility) for assistance with isothermal titration calorimetry; A. De Muyt and V. Borde for sharing information prior to publication; and members of the Corbett lab for helpful discussions.

FUNDING

National Institutes of Health/National Institute of General Medical Sciences [R01GM104141 to K.D.C.]; Ludwig Institute for Cancer Research. Funding for open access charge: National Institutes of Health.
Conflict of interest statement. None declared.

REFERENCES

1. Wang,S., Zickler,D., Kleckner,N. and Zhang,L. (2015) Meiotic crossover patterns: obligatory crossover, interference and homeostasis in a single process. *Cell Cycle*, **14**, 305–314.

2. Berchowitz,L.E. and Copenhaver,G. (2010) Genetic Interference: Don't stand so close to me. *Curr. Genom.*, **11**, 91–102.
3. Hassold,T., Hall,H. and Hunt,P. (2007) The origin of human aneuploidy: where we have been, where we are going. *Hum. Mol. Genet.*, **16**, R203–R208.
4. Hassold,T.J. and Hunt,P.A. (2001) To err (meiotically) is human: the genesis of human aneuploidy. *Nat. Rev. Genet.*, **2**, 280–291.
5. Mao-Draayer,Y., Galbraith,A.M., Pittman,D.L., Cool,M. and Malone,R.E. (1996) Analysis of meiotic recombination pathways in the yeast Saccharomyces cerevisiae. *Genetics*, **144**, 71–86.
6. Xu,L., Weiner,B.M. and Kleckner,N. (1997) Meiotic cells monitor the status of the interhomolog recombination complex. *Genes Dev.*, **11**, 106–118.
7. Peciña,A., Smith,K.N., Mézard,C., Murakami,H., Ohta,K. and Nicolas,A. (2002) Targeted stimulation of meiotic recombination. *Cell*, **111**, 173–184.
8. Schwacha,A. and Kleckner,N. (1997) Interhomolog bias during meiotic recombination: meiotic functions promote a highly differentiated interhomolog-only pathway. *Cell*, **90**, 1123–1135.
9. Woltering,D., Baumgartner,B., Bagchi,S., Larkin,B., Loidl,J., de los Santos,T. and Hollingsworth,N.M. (2000) Meiotic segregation, synapsis, and recombination checkpoint functions require physical interaction between the chromosomal proteins Red1p and Hop1p. *Mol. Cell. Biol.*, **20**, 6646–6658.
10. Blat,Y., Protacio,R.U., Hunter,N. and Kleckner,N. (2002) Physical and functional interactions among basic chromosome organizational features govern early steps of meiotic chiasma formation. *Cell*, **111**, 791–802.
11. Keeney,S., Giroux,C.N. and Kleckner,N. (1997) Meiosis-specific DNA double-strand breaks are catalyzed by Spo11, a member of a widely conserved protein family. *Cell*, **88**, 375–384.
12. Bishop,D.K., Park,D., Xu,L. and Kleckner,N. (1992) DMC1: a meiosis-specific yeast homolog of E. coli recA required for recombination, synaptonemal complex formation, and cell cycle progression. *Cell*, **69**, 439–456.
13. Cloud,V., Chan,Y.-L., Grubb,J., Budke,B. and Bishop,D.K. (2012) Rad51 is an accessory factor for Dmc1-mediated joint molecule formation during meiosis. *Science*, **337**, 1222–1225.
14. Niu,H., Wan,L., Baumgartner,B., Schaefer,D., Loidl,J. and Hollingsworth,N.M. (2005) Partner choice during meiosis is regulated by Hop1-promoted dimerization of Mek1. *Mol. Biol. Cell*, **16**, 5804–5818.
15. Subramanian,V.V., Macqueen,A.J., Vader,G., Shinohara,M., Sanchez,A., Borde,V., Shinohara,A. and Hochwagen,A. (2016) Chromosome synapsis alleviates Mek1-Dependent suppression of meiotic DNA repair. *PLoS Biol.*, **14**, e1002369.
16. Carballo,J.A., Johnson,A.L., Sedgwick,S.G. and Cha,R.S. (2008) Phosphorylation of the axial element protein Hop1 by Mec1/Tel1 ensures meiotic interhomolog recombination. *Cell*, **132**, 758–770.
17. Niu,H., Li,X., Job,E., Park,C., Moazed,D., Gygi,S.P. and Hollingsworth,N.M. (2007) Mek1 kinase is regulated to suppress double-strand break repair between sister chromatids during budding yeast meiosis. *Mol. Cell. Biol.*, **27**, 5456–5467.
18. Niu,H., Wan,L., Busygina,V., Kwon,Y., Allen,J.A., Li,X., Kunz,R.C., Kubota,K., Wang,B., Sung,P. *et al.* (2009) Regulation of meiotic recombination via Mek1-mediated Rad54 phosphorylation. *Mol. Cell*, **36**, 393–404.
19. Lao,J.P., Cloud,V., Huang,C.-C., Grubb,J., Thacker,D., Lee,C.-Y., Dresser,M.E., Hunter,N. and Bishop,D.K. (2013) Meiotic crossover control by concerted action of Rad51-Dmc1 in homolog template bias and robust homeostatic regulation. *PLos Genet.*, **9**, e1003978.
20. Kaur,H., De Muyt,A. and Lichten,M. (2015) Top3-Rmi1 DNA single-strand decatenase is integral to the formation and resolution of meiotic recombination intermediates. *Mol. Cell*, **57**, 583–594.
21. Oh,S.D., Lao,J.P., Hwang,P.Y.-H., Taylor,A.F., Smith,G.R. and Hunter,N. (2007) BLM ortholog, Sgs1, prevents aberrant crossing-over by suppressing formation of multichromatid joint molecules. *Cell*, **130**, 259–272.
22. De Muyt,A., Jessop,L., Kolar,E., Sourirajan,A., Chen,J., Dayani,Y. and Lichten,M. (2012) BLM helicase ortholog Sgs1 is a central regulator of meiotic recombination intermediate metabolism. *Mol. Cell*, **46**, 43–53.
23. Andersen,S.L. and Sekelsky,J. (2010) Meiotic versus mitotic recombination: two different routes for double-strand break repair: the different functions of meiotic versus mitotic DSB repair are reflected in different pathway usage and different outcomes. *Bioessays*, **32**, 1058–1066.
24. Allers,T. and Lichten,M. (2001) Differential timing and control of noncrossover and crossover recombination during meiosis. *Cell*, **106**, 47–57.
25. Hunter,N. and Kleckner,N. (2001) The single-end invasion: an asymmetric intermediate at the double-strand break to double-holliday junction transition of meiotic recombination. *Cell*, **106**, 59–70.
26. Schwacha,A. and Kleckner,N. (1995) Identification of double Holliday junctions as intermediates in meiotic recombination. *Cell*, **83**, 783–791.
27. Argueso,J.L., Wanat,J., Gemici,Z. and Alani,E. (2004) Competing crossover pathways act during meiosis in Saccharomyces cerevisiae. *Genetics*, **168**, 1805–1816.
28. Zakharyevich,K., Tang,S., Ma,Y. and Hunter,N. (2012) Delineation of joint molecule resolution pathways in meiosis identifies a crossover-specific resolvase. *Cell*, **149**, 334–347.
29. Blanco,M.G., Matos,J. and West,S.C. (2014) Dual control of Yen1 nuclease activity and cellular localization by Cdk and Cdc14 prevents genome instability. *Mol. Cell*, **54**, 94–106.
30. de los Santos,T., Hunter,N., Lee,C., Larkin,B., Loidl,J. and Hollingsworth,N.M. (2003) The Mus81/Mms4 endonuclease acts independently of double-Holliday junction resolution to promote a distinct subset of crossovers during meiosis in budding yeast. *Genetics*, **164**, 81–94.
31. Oh,S.D., Lao,J.P., Taylor,A.F., Smith,G.R. and Hunter,N. (2008) RecQ helicase, Sgs1, and XPF family endonuclease, Mus81-Mms4, resolve aberrant joint molecules during meiotic recombination. *Mol. Cell*, **31**, 324–336.
32. Lynn,A., Soucek,R. and Börner,G.V. (2007) ZMM proteins during meiosis: crossover artists at work. *Chromosome Res.*, **15**, 591–605.
33. Mazina,O.M., Mazin,A.V., Nakagawa,T., Kolodner,R.D. and Kowalczykowski,S.C. (2004) Saccharomyces cerevisiae Mer3 helicase stimulates 3′-5′ heteroduplex extension by Rad51; implications for crossover control in meiotic recombination. *Cell*, **117**, 47–56.
34. Snowden,T., Shim,K.-S., Schmutte,C., Acharya,S. and Fishel,R. (2008) hMSH4-hMSH5 adenosine nucleotide processing and interactions with homologous recombination machinery. *J. Biol. Chem.*, **283**, 145–154.
35. Snowden,T., Acharya,S., Butz,C., Berardini,M. and Fishel,R. (2004) hMSH4-hMSH5 recognizes Holliday Junctions and forms a meiosis-specific sliding clamp that embraces homologous chromosomes. *Mol. Cell*, **15**, 437–451.
36. Perry,J., Kleckner,N. and Börner,G.V. (2005) Bioinformatic analyses implicate the collaborating meiotic crossover/chiasma proteins Zip2, Zip3, and Spo22/Zip4 in ubiquitin labeling. *Proc. Natl Acad. Sci. U.S.A.*, **102**, 17594–17599.
37. Ahuja,J.S., Sandhu,R., Mainpal,R., Lawson,C., Henley,H., Hunt,P.A., Yanowitz,J.L. and Börner,G.V. (2017) Control of meiotic pairing and recombination by chromosomally tethered 26S proteasome. *Science*, **355**, 408–411.
38. Rao,H.B.D.P., Qiao,H., Bhatt,S.K., Bailey,L.R.J., Tran,H.D., Bourne,S.L., Qiu,W., Deshpande,A., Sharma,A.N., Beebout,C.J. *et al.* (2017) A SUMO-ubiquitin relay recruits proteasomes to chromosome axes to regulate meiotic recombination. *Science*, **355**, 403–407.
39. Sym,M., Engebrecht,J.A. and Roeder,G.S. (1993) ZIP1 is a synaptonemal complex protein required for meiotic chromosome synapsis. *Cell*, **72**, 365–378.
40. Dong,H. and Roeder,G.S. (2000) Organization of the yeast Zip1 protein within the central region of the synaptonemal complex. *J. Cell Biol.*, **148**, 417–426.
41. Zickler,D. and Kleckner,N. (1999) Meiotic chromosomes: integrating structure and function. *Annu. Rev. Genet.*, **33**, 603–754.
42. Chen,C., Jomaa,A., Ortega,J. and Alani,E.E. (2014) Pch2 is a hexameric ring ATPase that remodels the chromosome axis protein Hop1. *Proc. Natl. Acad. Sci. U.S.A.*, **111**, E44–E53.
43. Joshi,N., Barot,A., Jamison,C. and Börner,G.V. (2009) Pch2 links chromosome axis remodeling at future crossover sites and crossover distribution during yeast meiosis. *PLos Genet.*, **5**, e1000557.
44. Borner,G.V., Barot,A. and Kleckner,N. (2008) Yeast Pch2 promotes domainal axis organization, timely recombination progression, and

arrest of defective recombinosomes during meiosis. *Proc. Natl. Acad. Sci. U.S.A.*, **105**, 3327–3332.
45. Ye,Q., Kim,D.H., Dereli,I., Rosenberg,S.C., Hagemann,G., Herzog,F., Toth,A., Cleveland,D.W. and Corbett,K.D. (2017) The AAA+ ATPase TRIP13 remodels HORMA domains through N-terminal engagement and unfolding. *EMBO J.*, **36**, 2419–2434.
46. Fung,J.C., Rockmill,B., Odell,M. and Roeder,G.S. (2004) Imposition of crossover interference through the nonrandom distribution of synapsis initiation complexes. *Cell*, **116**, 795–802.
47. Chua,P.R. and Roeder,G.S. (1998) Zip2, a meiosis-specific protein required for the initiation of chromosome synapsis. *Cell*, **93**, 349–359.
48. Tsubouchi,T., Zhao,H. and Roeder,G.S. (2006) The meiosis-specific zip4 protein regulates crossover distribution by promoting synaptonemal complex formation together with zip2. *Dev. Cell*, **10**, 809–819.
49. Shinohara,M., Oh,S.D., Hunter,N. and Shinohara,A. (2008) Crossover assurance and crossover interference are distinctly regulated by the ZMM proteins during yeast meiosis. *Nat. Genet.*, **40**, 299–309.
50. Malavasic,M.J. and Elder,R.T. (1990) Complementary transcripts from two genes necessary for normal meiosis in the yeast Saccharomyces cerevisiae. *Mol. Cell. Biol.*, **10**, 2809–2819.
51. Chen,S.Y., Tsubouchi,T., Rockmill,B., Sandler,J.S., Richards,D.R., Vader,G., Hochwagen,A., Roeder,G.S. and Fung,J.C. (2008) Global analysis of the meiotic crossover landscape. *Dev. Cell*, **15**, 401–415.
52. Börner,G.V., Kleckner,N. and Hunter,N. (2004) Crossover/noncrossover differentiation, synaptonemal complex formation, and regulatory surveillance at the leptotene/zygotene transition of meiosis. *Cell*, **117**, 29–45.
53. Macaisne,N., Novatchkova,M., Peirera,L., Vezon,D., Jolivet,S., Froger,N., Chelysheva,L., Grelon,M. and Mercier,R. (2008) SHOC1, an XPF Endonuclease-Related protein, is essential for the formation of class I meiotic crossovers. *Curr. Biol.*, **18**, 1432–1437.
54. Guiraldelli,M.F., Felberg,A., Almeida,L.P., Parikh,A., de Castro,R.O. and Pezza,R.J. (2018) SHOC1 is a ERCC4-(HhH)2-like protein, integral to the formation of crossover recombination intermediates during mammalian meiosis. *PLos Genet.*, **14**, e1007381.
55. De Muyt,A., Pyatnitskaya,A., Andréani,J., Ranjha,L., Ramus,C., Laureau,R., Fernandez-Vega,A., Holoch,D., Girard,E., Govin,J. *et al.* (2018) A meiotic XPF-ERCC1-like complex recognizes joint molecule recombination intermediates to promote crossover formation. *Genes Dev.*, **32**, 283–296.
56. Macaisne,N., Vignard,J. and Mercier,R. (2011) SHOC1 and PTD form an XPF-ERCC1-like complex that is required for formation of class I crossovers. *J. Cell Sci.*, **124**, 2687–2691.
57. Yang,H., Zhang,T., Tao,Y., Wang,F., Tong,L. and Ding,J. (2013) Structural insights into the functions of the FANCM-FAAP24 complex in DNA repair. *Nucleic Acids Res.*, **41**, 10573–10583.
58. Gibson,D.G., Young,L., Chuang,R.-Y., Venter,J.C., Hutchison,C.A. and Smith,H.O. (2009) Enzymatic assembly of DNA molecules up to several hundred kilobases. *Nat. Methods*, **6**, 343–345.
59. Goldschmidt,L., Cooper,D.R., Derewenda,Z.S. and Eisenberg,D. (2007) Toward rational protein crystallization: a Web server for the design of crystallizable protein variants. *Protein Sci.*, **16**, 1569–1576.
60. Kabsch,W. (2010) XDS. *Acta Crystallogr. D. Biol. Crystallogr.*, **66**, 125–132.
61. Winn,M.D., Ballard,C.C., Cowtan,K.D., Dodson,E.J., Emsley,P., Evans,P.R., Keegan,R.M., Krissinel,E.B., Leslie,A.G.W., McCoy,A. *et al.* (2011) Overview of the CCP4 suite and current developments. *Acta Crystallogr. D. Biol. Crystallogr.*, **67**, 235–242.
62. Pape,T. and Schneider,T.R.IUCr (2004) HKL2MAP: a graphical user interface for macromolecular phasing with SHELX programs. *J. Appl. Crystallogr.*, **37**, 843–844.
63. Sheldrick,G.M. (2010) Experimental phasing with SHELXC/D/E: combining chain tracing with density modification. *Acta Crystallogr. D. Biol. Crystallogr.*, **66**, 479–485.
64. Terwilliger,T.C., Adams,P.D., Read,R.J., McCoy,A.J., Moriarty,N.W., Grosse-Kunstleve,R.W., Afonine,P.V., Zwart,P.H. and Hung,L.W. (2009) Decision-making in structure solution using Bayesian estimates of map quality: the PHENIX AutoSol wizard. *Acta Crystallogr. D. Biol. Crystallogr.*, **65**, 582–601.
65. Adams,P.D., Afonine,P.V., Bunkóczi,G., Chen,V.B., Davis,I.W., Echols,N., Headd,J.J., Hung,L.W., Kapral,G.J., Grosse-Kunstleve,R.W. *et al.* (2010) PHENIX: a comprehensive Python-based system for macromolecular structure solution. *Acta Crystallogr. D. Biol. Crystallogr.*, **66**, 213–221.
66. McCoy,A.J., Grosse-Kunstleve,R.W., Adams,P.D., Winn,M.D., Storoni,L.C. and Read,R.J. (2007) Phaser crystallographic software. *J. Appl. Crystallogr.*, **40**, 658–674.
67. Terwilliger,T.C. (2000) Maximum-likelihood density modification. *Acta Crystallogr. D. Biol. Crystallogr.*, **56**, 965–972.
68. Terwilliger,T.C. (2003) Automated main-chain model building by template matching and iterative fragment extension. *Acta Crystallogr. D. Biol. Crystallogr.*, **59**, 38–44.
69. Emsley,P., Lohkamp,B., Scott,W.G. and Cowtan,K. (2010) Features and development of Coot. *Acta Crystallogr. D. Biol. Crystallogr.*, **66**, 486–501.
70. Afonine,P.V., Grosse-Kunstleve,R.W., Echols,N., Headd,J.J., Moriarty,N.W., Mustyakimov,M., Terwilliger,T.C., Urzhumtsev,A., Zwart,P.H., Adams,P.D. *et al.* (2012) Towards automated crystallographic structure refinement with phenix.refine. *Acta Crystallogr. D. Biol. Crystallogr.*, **68**, 352–367.
71. Bateman,R., Rauh,D. and Shokat,K.M. (2007) Glutathione traps formaldehyde by formation of a bicyclo[4.4.1]undecane adduct. *Org. Biomol. Chem.*, **5**, 3363–3367.
72. Metz,B., Kersten,G.F.A., Hoogerhout,P., Brugghe,H.F., Timmermans,H.A.M., de Jong,A., Meiring,H., Hove ten,J., Hennink,W.E., Crommelin,D.J.A. *et al.* (2004) Identification of formaldehyde-induced modifications in proteins: reactions with model peptides. *J. Biol. Chem.*, **279**, 6235–6243.
73. Jurrus,E., Engel,D., Star,K., Monson,K., Brandi,J., Felberg,L.E., Brookes,D.H., Wilson,L., Chen,J., Liles,K. *et al.* (2018) Improvements to the APBS biomolecular solvation software suite. *Protein Sci.*, **27**, 112–128.
74. Walter,T.S., Meier,C., Assenberg,R., Au,K.-F., Ren,J., Verma,A., Nettleship,J.E., Owens,R.J., Stuart,D.I. and Grimes,J.M. (2006) Lysine methylation as a routine rescue strategy for protein crystallization. *Structure*, **14**, 1617–1622.
75. Kim,Y., Quartey,P., Li,H., Volkart,L., Hatzos,C., Chang,C., Nocek,B., Cuff,M., Osipiuk,J., Tan,K. *et al.* (2008) Large-scale evaluation of protein reductive methylation for improving protein crystallization. *Nat. Methods*, **5**, 853–854.
76. Derewenda,Z.S. (2004) Rational protein crystallization by mutational surface engineering. *Structure*, **12**, 529–535.
77. Aravind,L., Walker,D.R. and Koonin,E.V. (1999) Conserved domains in DNA repair proteins and evolution of repair systems. *Nucleic. Acids. Res.*, **27**, 1223–1242.
78. Ciccia,A., McDonald,N. and West,S.C. (2008) Structural and functional relationships of the XPF/MUS81 family of proteins. *Annu. Rev. Biochem.*, **77**, 259–287.
79. Newman,M., Murray-Rust,J., Lally,J., Rudolf,J., Fadden,A., Knowles,P.P., White,M.F. and McDonald,N.Q. (2005) Structure of an XPF endonuclease with and without DNA suggests a model for substrate recognition. *EMBO J.*, **24**, 895–905.
80. Nishino,T., Komori,K., Ishino,Y. and Morikawa,K. (2003) X-ray and biochemical anatomy of an archaeal XPF/Rad1/Mus81 family nuclease: similarity between its endonuclease domain and restriction enzymes. *Structure*, **11**, 445–457.
81. Marsolier-Kergoat,M.-C., Khan,M.M., Schott,J., Zhu,X. and Llorente,B. (2018) Mechanistic view and genetic control of DNA recombination during meiosis. *Mol. Cell*, **70**, 9–20.
82. Das,D., Folkers,G.E., van Dijk,M., Jaspers,N.G.J., Hoeijmakers,J.H.J., Kaptein,R. and Boelens,R. (2012) The structure of the XPF-ssDNA complex underscores the distinct roles of the XPF and ERCC1 helix- hairpin-helix domains in ss/ds DNA recognition. *Structure*, **20**, 667–675.
83. Gwon,G.H., Jo,A., Baek,K., Jin,K.S., Fu,Y., Lee,J.-B., Kim,Y. and Cho,Y. (2014) Crystal structures of the structure-selective nuclease Mus81-Eme1 bound to flap DNA substrates. *EMBO J.*, **33**, 1061–1072.
84. Crown,K.N., McMahan,S. and Sekelsky,J. (2014) Eliminating both canonical and short-patch mismatch repair in Drosophila melanogaster suggests a new meiotic recombination model. *PLos Genet.*, **10**, e1004583.